

Barrier crossing driven by Lévy noise: Universality and the Role of Noise Intensity

Aleksei V. Chechkin,¹ Oleksii Yu. Sliusarenko,¹ Ralf Metzler,^{2,3} and Joseph Klafter⁴

¹*Institute for Theoretical Physics NSC KIPT, Akademicheskaya st.1, 61108 Kharkov, Ukraine*

²*Dept of Physics, University of Ottawa - 150 Louis Pasteur, Ottawa, ON, K1N 6N5, Canada*

³*NORDITA—Nordic Institute for Theoretical Physics, Blegdamsvej 17, 2100 Copenhagen Ø, Denmark*

⁴*School of Chemistry, Tel Aviv University, Ramat Aviv, Tel Aviv 69978, Israel*

(Dated: 20th March 2018)

We study the barrier crossing of a particle driven by white symmetric Lévy noise of index α and intensity D for three different generic types of potentials: (a) a bistable potential; (b) a metastable potential; and (c) a truncated harmonic potential. For the low noise intensity regime we recover the previously proposed algebraic dependence on D of the characteristic escape time, $T_{\text{esc}} \simeq C(\alpha)/D^{\mu(\alpha)}$, where $C(\alpha)$ is a coefficient. It is shown that the exponent $\mu(\alpha)$ remains approximately constant, $\mu \approx 1$ for $0 < \alpha < 2$; at $\alpha = 2$ the power-law form of T_{esc} changes into the known exponential dependence on $1/D$; it exhibits a divergence-like behavior as α approaches 2. In this regime we observe a monotonous increase of the escape time T_{esc} with increasing α (keeping the noise intensity D constant). The probability density of the escape time decays exponentially. In addition, for low noise intensities the escape times correspond to barrier crossing by multiple Lévy steps. For high noise intensities, the escape time curves collapse for all values of α . At intermediate noise intensities, the escape time exhibits non-monotonic dependence on the index α , while still retaining the exponential form of the escape time density.

PACS numbers: 05.40.Fb, 02.50.-Ey, 82.20.-w

I. INTRODUCTION

In his seminal paper [1], Kramers proposed to model chemical reaction rates as the diffusion of a Brownian particle, initially located in a potential well, across a potential barrier of finite height. Meanwhile, Kramers' theory has been applied to a much more general range of processes associated with the barrier crossing of a physical entity experiencing random kicks fuelled by its contact to a thermal bath [2, 3, 4, 5].

Since Kramers' solution numerous different ways have been reported to access the barrier crossing problem, in particular, to find the mathematically most convenient formulation, compare, for instance, Refs. [3, 4, 5, 6]. The result for the characteristic escape time reads [7]

$$T_{\text{esc}} = \frac{2\pi \exp([U(x_{\text{max}}) - U(x_{\text{min}})]/D)}{\sqrt{|U''(x_{\text{min}})| |U''(x_{\text{max}})|}} \quad (1)$$

where $U(x)$ is the dimensionless potential, a prime stands for the derivative with respect to the coordinate x ; x_{min} and x_{max} are the points, where the potential $U(x)$ attains its minimum and maximum, respectively; and D is the diffusion coefficient (noise intensity) of the diffusing particle, stemming from its coupling to the heat bath. Eq. (1) is based on the assumption that the barrier is high (or equivalently, the noise intensity is low), and there exists a constant probability flux across the barrier maximum.

Random processes in complex systems frequently violate the rules of Brownian motion. Thus, the presence of static or dynamic disorder might give rise to memory effects causing subdiffusion [8, 9], and possible deviations from standard exponential relaxation [10, 11].

The barrier crossing in the presence of long-range memory effects was, inter alia, modeled in terms of a generalized Langevin equation [12, 13], or via a subdiffusive fractional kinetic approach with Mittag-Leffler survival [14, 15]. Subdiffusion is usually associated with a long-tailed waiting time distribution $\psi(t) \sim A_{\gamma} \tau^{\gamma} / t^{1+\gamma}$ with $0 < \gamma < 1$ rendering the resulting continuous time random walk process semi-Markovian, its hallmark being the power-law time-dependence $\langle x^2 \rangle \propto K_{\gamma} t^{\gamma}$ of the mean-squared displacement in absence of an external potential [8, 9, 16].

While in subdiffusion the waiting time between successive jump events becomes modified such that the mean waiting time $\int_0^{\infty} t\psi(t)dt$ diverges and consequently no natural time scale separating microscopic and macroscopic events exists, the distribution of the lengths of individual jumps is narrow. The converse is true for Lévy flights: Here, the lengths of the jumps are distributed according to the long-tailed jump length distribution

$$\lambda(x) \sim \frac{A_{\alpha} \sigma^{\alpha}}{|x|^{1+\alpha}} \quad (2)$$

with $0 < \alpha < 2$ [8, 15, 17, 18]. Thus, the variance $\int_{-\infty}^{\infty} x^2 \lambda(x) dx$ of the jump lengths diverges. Such power-law forms of the jump lengths have been recognized in a wide number of fields [9]. Prominent examples for such genuine Lévy flights are known from noise patterns in plasma devices [19], and from random walks of particles or excitations along a fastly folding polymer, where the walker is allowed to cross the small gap between two segments of the chain, that are close by in the embedding space due to polymer looping [20]. In the latter case, the exponent α is in fact related to the critical exponents of the polymer chain. Further examples come from fluctua-

tions in energy space in small systems [21, 22], and from paleoclimatic time series [23].

From a mathematical point of view the occurrence of long-tailed distributions appears quite natural due to the Lévy-Gnedenko generalized central limit theorem [24, 25]. Indeed, the tails of probability densities of the type of $\lambda(x)$, Eq. (2), are obtained from the characteristic function of a symmetric α -stable distribution of the form

$$\lambda(k) \equiv \mathcal{F}\{\lambda(x)\} = \int_{-\infty}^{\infty} e^{ikx} \lambda(x) dx = \exp(-c|k|^\alpha), \quad (3)$$

where $c > 0$. The power-law asymptotics at large $|x|$, Eq. (2), appear immediately from the expansion of the characteristic function Eq. (3) in the limit of small k .

An important question arises when replacing the Brownian particle in a barrier crossing process by a particle executing Lévy flights. This situation can be modelled by a particle subject to Lévy stable noise, on the level of the Langevin equation. First steps in this direction of addressing have been taken, as reported in Refs. [26, 27, 28, 29]. In the present work, we report extended simulation results for the usually studied case of low noise strength D , observing a pronounced step-like behavior of the dependence of the exponent μ on the Lévy index α . We also explore the case of intermediate and high noise strength, finding a quite rich behavior in the parameter space, including an optimum α for the escape time.

II. UNDERLYING LANGEVIN EQUATION

We start from the Langevin equation for a particle embedded in an external potential field and subjected to a random noise,

$$\frac{dx(t)}{dt} = -\frac{1}{m\gamma} \frac{dU(x)}{dx} + \xi_\alpha(t), \quad (4)$$

where $x(t)$ is the dynamic variable (particle position), m the mass, γ the friction constant, and $U(x)$ an external potential. The noise $\xi_\alpha(t)$ is a white, symmetric α -stable noise. Eq. (4) is understood in the following way [30]. Integrating Eq. (4) over the interval $[t, t + \Delta t]$, we obtain

$$x(t + \Delta t) - x(t) = -\frac{1}{m\gamma} \int_t^{t+\Delta t} \frac{dU(x(t'))}{dx} dt' + L_{\alpha,D}(\Delta t), \quad (5)$$

where

$$L_{\alpha,D}(\Delta t) = \int_t^{t+\Delta t} \xi_{\alpha,D}(t') dt' \quad (6)$$

is an α -stable process with stationary independent increments and characteristic function

$$p_L(k, \Delta t) = \exp(-D|k|^\alpha \Delta t). \quad (7)$$

D is the intensity of the Lévy noise. With the use of Eqs. (6) and (7) it is straightforward to show [30] that the discrete time representation of Eq. (5) at times $t_n = n\delta t$, $n = 0, 1, 2, \dots$ for sufficiently small time step δt is

$$x_{n+1} - x_n = -\frac{1}{m\gamma} \frac{dU(x_n)}{dx} \delta t + (D\delta t)^{1/\alpha} \xi_{\alpha,1}(n), \quad (8)$$

where $\{\xi_{\alpha,1}(n)\}$ is a set of random variables possessing Lévy stable distribution $\lambda(x)$ with the characteristic function (3) and $c = 1$.

III. SIMULATIONS RESULTS

Before addressing the barrier crossing problem in the presence of Lévy stable noise analytically below, we present results from extensive simulations. In these simulations, we employ three types of potential profiles: bistable, metastable, and truncated harmonic potentials (see Fig.1) defined as follows:

$$U_1(x) = -g_1 \frac{x^2}{2} + g_2 \frac{x^4}{4}; \quad (9a)$$

$$U_2(x) = -g_1 \frac{x^3}{3} + g_2 x \quad (9b)$$

$$U_3(x) = \begin{cases} g_1 x^2/2, & -L \leq x \leq L \\ 0, & |x| > L \end{cases}. \quad (9c)$$

Let us turn to dimensionless variables. To this end we substitute $x \rightarrow x/\tilde{x}$, $t \rightarrow t/\tilde{t}$, and $D \rightarrow D/\tilde{D}$ into the discrete time Langevin equation (8), and choose the appropriate constants for rescaling, \tilde{x} , \tilde{t} , and \tilde{D} , for each potential type. Taking into account that $\xi_\alpha(t/\tilde{t}) = \tilde{t}^{1-1/\alpha} \xi_\alpha(t)$ [30], we find

$$\tilde{x} = \sqrt{\frac{g_2}{g_1}}, \tilde{t} = \frac{g_1}{m\gamma}, \tilde{D} = \frac{m\gamma}{g_1} \left(\frac{g_2}{g_1}\right)^{\alpha/2}; \quad (10a)$$

$$\tilde{x} = \sqrt{\frac{g_1}{g_2}}, \tilde{t} = \frac{\sqrt{g_1 g_2}}{m\gamma}, \tilde{D} = \frac{m\gamma}{\sqrt{g_1 g_2}} \left(\frac{g_1}{g_2}\right)^{\alpha/2} \quad (10b)$$

$$\tilde{x} = L, \frac{\tilde{x}^\alpha}{\tilde{D}} = \tilde{t} = \frac{m\gamma}{g_1}, \quad (10c)$$

respectively. In terms of these rescaled variables the discrete time Langevin equation (8) reads

$$x_{n+1} - x_n = -\frac{dU(x_n)}{dx} \delta t + (D\delta t)^{1/\alpha} \xi_{\alpha,1}(n), \quad (11)$$

where the potential $U(x_n)$ refers to, respectively, U_1 , U_2 , or U_3 from Eqs. (9), with $g_1 = g_2 = L = 1$.

In the simulations, for each type of the potential the particle starts from the bottom of the potential well. The adsorbing boundary is located: (i) for the bistable potential in the saddle point $x = 0$; (ii) for the metastable potential far to the right of the saddle point, at $x = 10$; and (iii) for the truncated harmonic potential at the boundaries, $|x| = 1$. The process defined by Eq. (11) is repeated

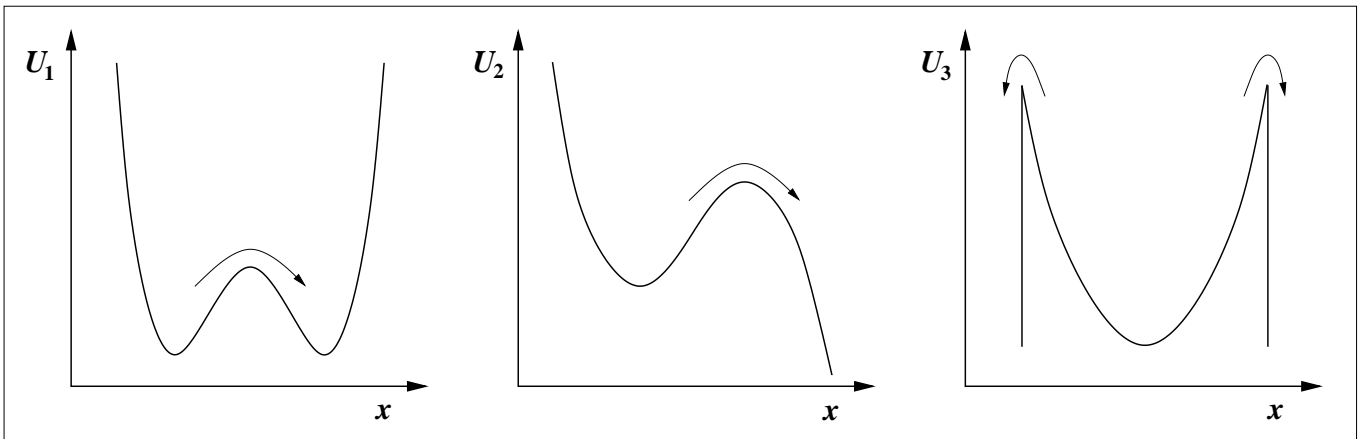


Figure 1: The three types of potential profiles U_1 (bistable potential), U_2 (metastable potential), and U_3 (truncated harmonic potential) considered in the simulations; for $g_1, g_2, L > 0$.

until the particle reaches, or crosses the adsorbing boundary; then the process in Eq. (11) is restarted. This procedure is performed 100,000 times, for fixed D and α , and the mean escape time is then calculated [31].

The mean escape times T_{esc} of the diffusing particle as function of noise intensity D for the three potential profiles are shown in Fig. 2 for different values of α ranging from 0.1 to 2 [32]. It is clear that the curves for $\alpha < 2$ obey a different law in comparison to their Gaussian counterpart. We observe three different regimes for the dependence of T_{esc} on the Lévy noise parameters, which can be classified by the value of noise intensity. Let us discuss these regimes in detail.

A. Low noise intensity regime

In this regime, instead of an exponential dependence on $1/D$, the curves shown in Fig. 2 display a power-law asymptotic behavior of the mean escape time

$$T_{\text{esc}}(\alpha, D) = \frac{C(\alpha)}{D^{\mu(\alpha)}}. \quad (12)$$

Further analysis of the data plotted in Fig. 2 allows us to determine the dependencies of the power law exponent $\mu(\alpha)$ and coefficient $C(\alpha)$ on the Lévy index α (see Fig. 3). The exponent $\mu(\alpha)$ is approximately unity up to $\alpha \approx 1.5$. The dependence of $C(\alpha)$ for the first two potential types possesses a weak inflection at small α . Note that for fixed noise strength D , the dependence of T_{esc} on the Lévy index α is monotonic.

Let us now turn to the probability density function (PDF) $p(t)$ of the escape times. We use again our simulation scheme to obtain $p(t)$ from the Langevin equation (11), but now for each fixed values of α and D we collect 200,000 escape events, which are not averaged but processed with a simple routine, that constructs the PDF. The results for the three potentials from Fig.1 are shown in Fig. 4 [34]. It is imminently clear that in all three

cases and for all α (including the Gaussian case, $\alpha = 2$) the exponential decay pattern

$$p(t) = \frac{1}{T} \exp\left(-\frac{t}{T}\right) \quad (13)$$

is nicely obeyed, in agreement with the findings from previous simulations studies [23, 28, 29], as well as with the analytical results reported in Ref. [26].

Relation (13) allows us to extract the mean escape time T_{esc} independently from our previous results in Fig. 2, in two different ways. Namely, we define

$$T_{\text{esc}} = \frac{1}{p(0)} \equiv T_1; \quad (14)$$

alternatively, we determine

$$T_{\text{esc}} = -\left(\frac{d \ln p(t)}{dt}\right)^{-1} \equiv T_2. \quad (15)$$

These two ways to determine T_{esc} are intrinsically different, T_1 depending on the extrapolation of the fitted exponential behavior to $t = 0$, whereas T_2 is determined through the slope in the logarithmic versus linear plot. Tab. I shows the results for T_1 and T_2 along with the values of T_{esc} obtained directly from the simulations results in Figs. 2. Indeed, the value of T_2 is consistently closer to T_{esc} than T_1 . Overall, however, the agreement is very good (better than 1.5 per cent).

B. High and intermediate noise intensity regimes

We consider these two regimes for the case of the truncated harmonic potential as example, compare to the bottom graph in Fig.2. The two other cases, bistable and metastable potentials, demonstrate similar behavior. When the noise intensity D increases beyond the low noise limit, in which the curves exhibit a linear dependence and are almost parallel, the various curves for

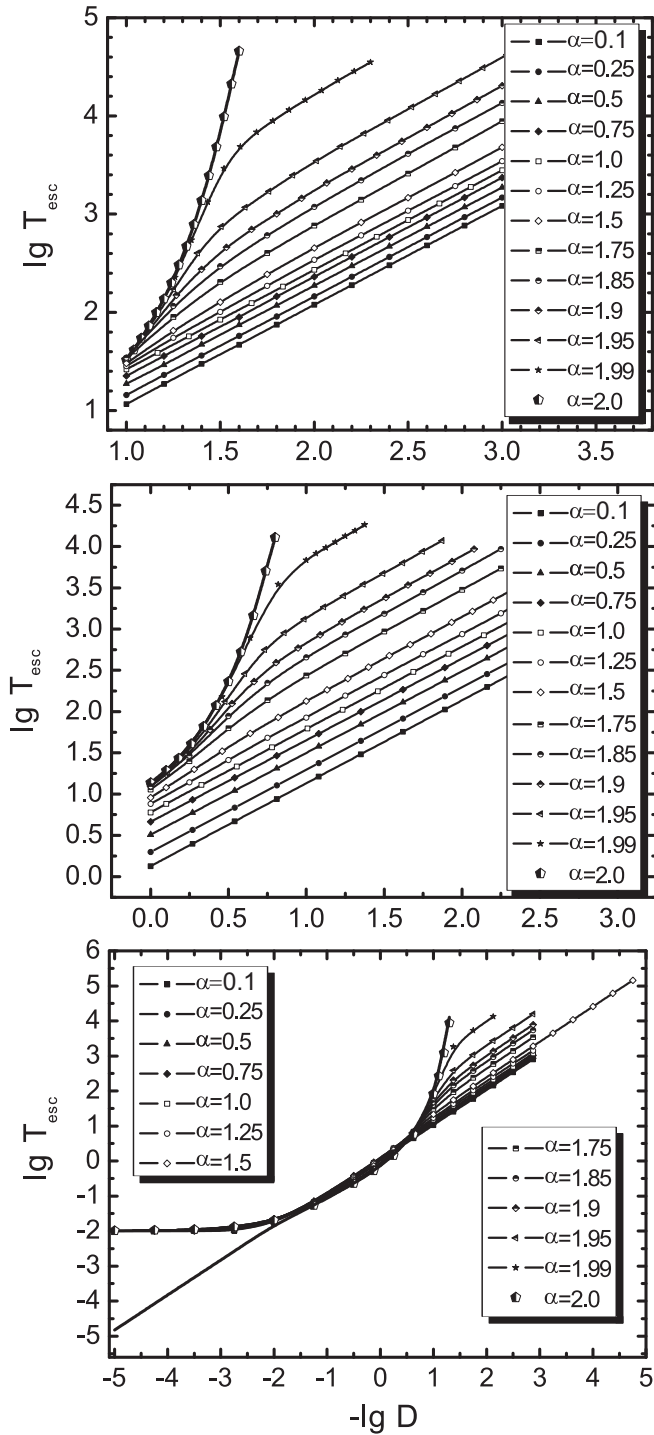


Figure 2: Mean escape times as function of noise intensity D for the bistable (top), metastable (middle), and truncated harmonic potentials (bottom).

the escape time show a tendency to collapse. This is the intermediate noise intensity regime, which for the truncated harmonic potential lies approximately in the range $-2 < -\lg D < 1$. Here, we observe that T_{esc} demonstrates very weak dependence on the Lévy index, in comparison with the low intensity regime. The ex-

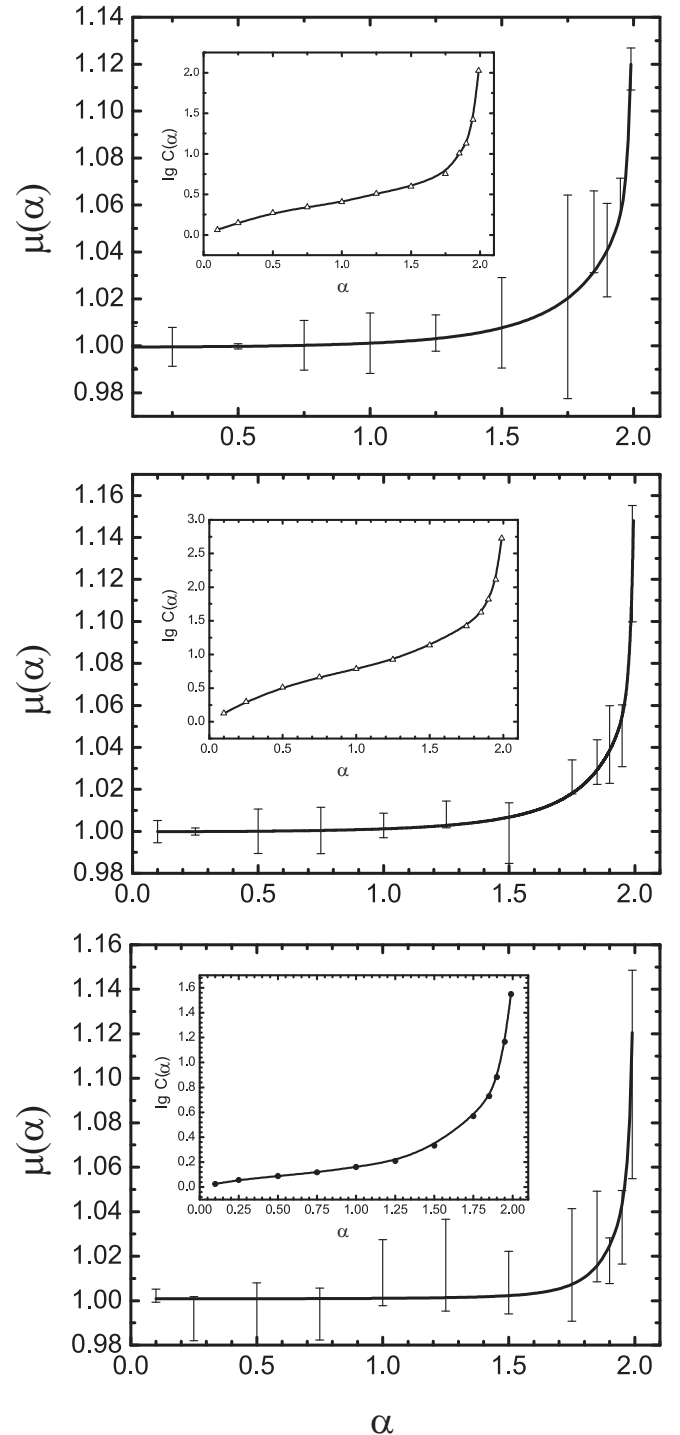


Figure 3: Dependencies of $\mu(\alpha)$ and $C(\alpha)$ for the bistable (top), metastable (middle) and truncated harmonic (bottom) potentials. See text.

planation is the following. Contrary to the weak noise intensity regime, where the tail of the Lévy noise distribution plays a decisive role in the escape process (less frequent but high amplitude noise spikes, that is, govern the barrier crossing), here the main role in the process, due to the higher intensities, passes on to the central part

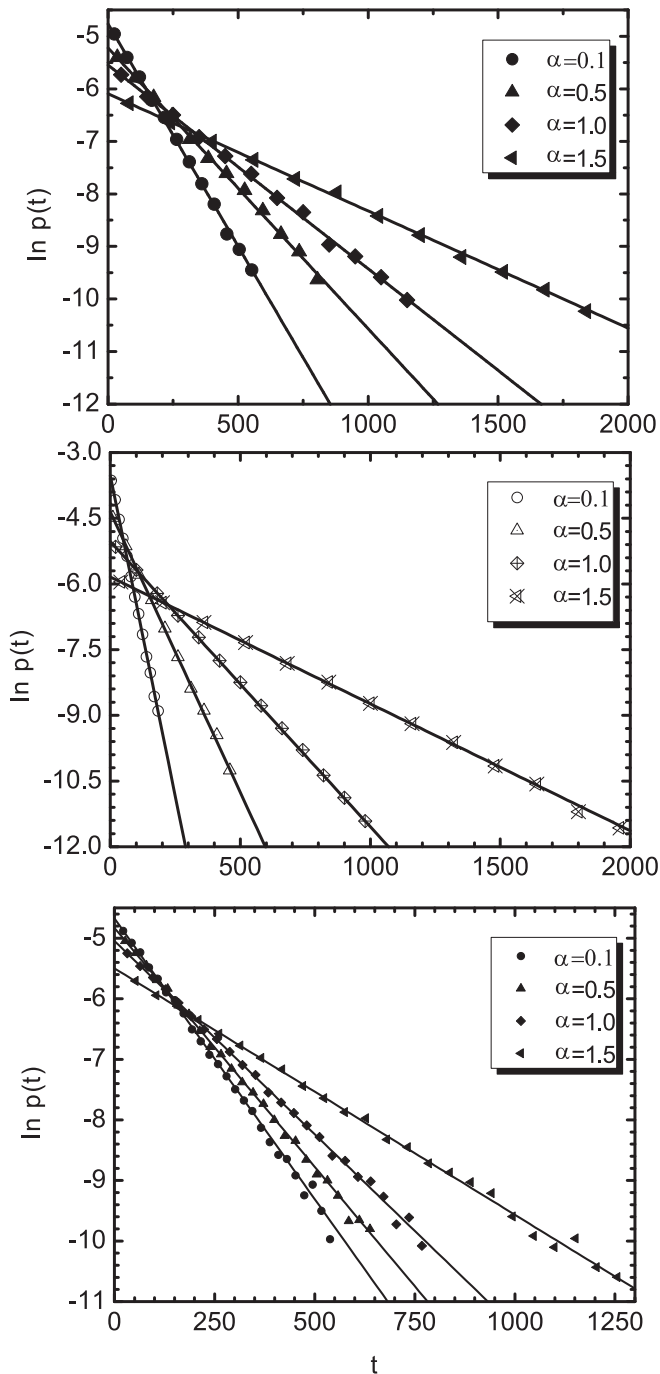


Figure 4: Escape time probability density functions in dependence of time for the bistable (top), metastable (middle) and truncated harmonic (bottom) potentials. In the log versus lin plot, the exponential dependence is obvious.

of the distribution. Since all stable distributions, including the Gaussian, have central parts which are of similar shape, the α -dependence of the escape time becomes weaker. Furthermore, in the intermediate region we observe a non-monotonic dependence of T_{esc} versus α , examples for three values of D taken from the intermediate regime are shown in Fig. 5. This weak non-monotonicity

First potential type, $D = 10^{-2.0}$			
α	T_{esc}	T_1	T_2
0.1	119.7	117.4	118.1
0.5	187.1	185.1	187.1
1.0	260.8	257.1	258.2
1.5	446.5	443.4	448.4
Second potential type, $D = 10^{-1.4}$			
α	T_{esc}	T_1	T_2
0.1	34.2	33.9	34.1
0.5	78.3	77.8	78.1
1.0	153.7	153.0	153.5
1.5	346.6	342.9	344.9
Third potential type, $D = 10^{-2.0}$			
α	T_{esc}	T_1	T_2
0.1	108.2	107.1	107.9
0.5	127.4	125.4	126.8
1.0	159.1	155.7	156.7
1.5	250.2	244.6	245.9

Table I: Mean escape times, obtained using three separate methods: T_{esc} is determined directly from the simulations producing Fig. 2, while T_1 and T_2 are defined in Eqs. (14) and (15), respectively.

most likely reflects minor differences in the shapes of the distribution of the noise ξ_α in the central part (relative to the much more pronounced differences in the tails of these PDFs). This point will be investigated in more detail in a forthcoming paper. Another important feature of the intermediate regime is that the PDF of the escape times remains exponential. This is clearly seen in Fig. 6. In that figure, one can also recognize that for $\alpha = 0.1$ and 1.25, as well as $\alpha = 0.75$ and 1.0 are almost coinciding.

In Fig. 5 we also show the dependence of the mean escape time on the time increment δt used in our simulations, showing a much higher sensitivity to the particular value chosen for δt than in the regime of low noise strength. This is intuitively clear, as now the process is terminated after few jumps only. As seen in Fig. 5, for increasingly small δt , the shown curves converge. Note, however, that the weak non-monotonicity of the escape time on α is preserved for all δt .

When the noise intensity D is increased further, the intermediate regime turns over to the high noise intensity regime. Here, all the curves for the escape time T_{esc} collapse into a single curve, that approaches the constant value $T_{\text{esc}} = 10^{-2}$, independent of D . Noting that in our simulation scheme the time step $\delta t = 10^{-2}$ is used, we conclude that in the region of high noise intensity the particles reach the boundary in a single jump. We confirmed this conclusion by taking different values of the time step, observing that, whereas the picture in the low and intermediate regions changes negligibly, in the high intensity regime the collapsed curves again approach the

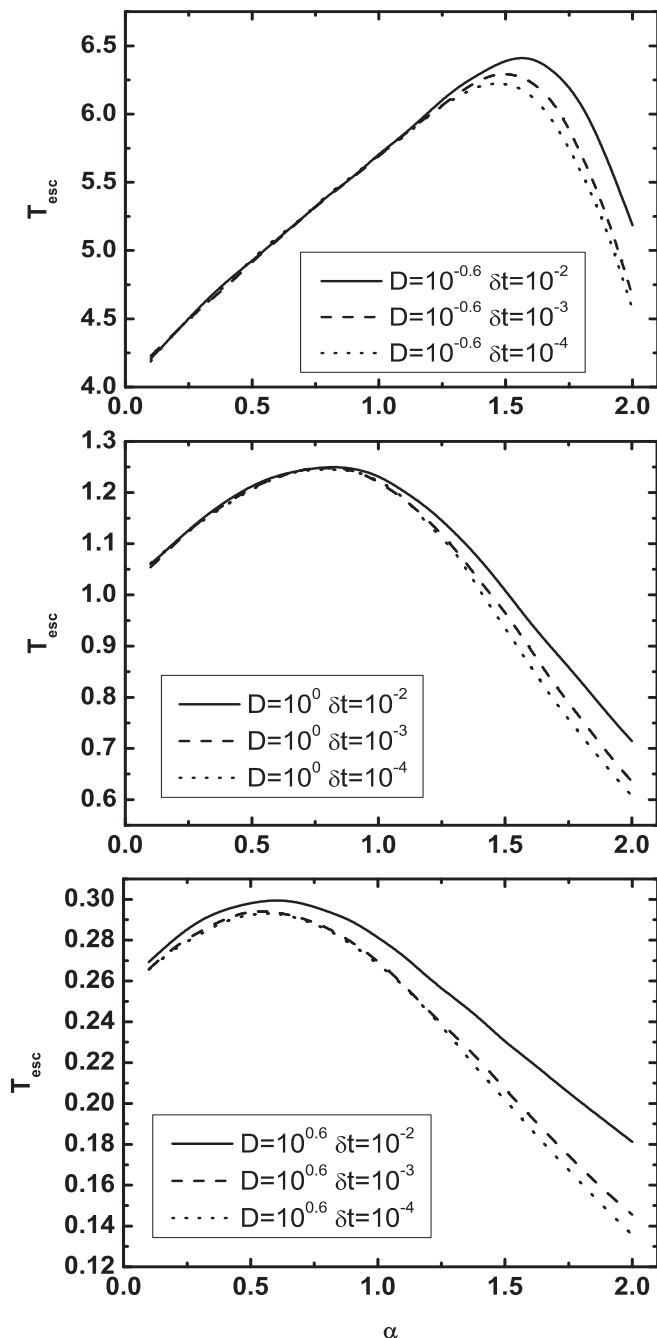


Figure 5: Dependence of mean escape time T_{esc} on Lévy index α , for various noise intensities D in the intermediate regime. For these results we used the truncated harmonic potential. The weak dependence on the time increment δt of the simulation is discussed in the text.

value of T_{esc} equal to a single time step.

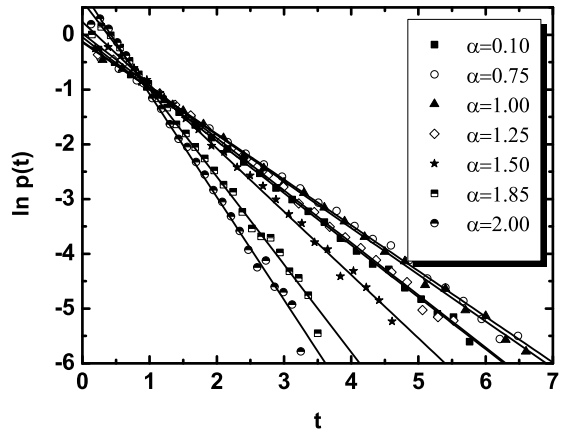


Figure 6: Escape time PDF for the intermediate noise strength, with $D = 1$. Note that the curves for $\alpha = 0.1$ and 1.25 , as well as $\alpha = 0.75$ and 1.0 are almost coincide, pointing at a weak inversion of the α -dependence.

IV. ANALYTICAL RESULTS FOR THE CAUCHY CASE, $\alpha = 1$

A standard approach to the classical barrier crossing problem in the presence of Gaussian white noise is based on the stationary flux approximation assuming that the probability current across the barrier is constant. This is equivalent to requiring that the barrier is high in comparison to thermal energy, or the noise intensity D low. The stationary flux approximation is widely used for the classical Kramers problem [1, 3, 6, 7, 35]. Here, we extend this assumption to the case of white Lévy noise, and obtain analytical results for the Cauchy case, $\alpha = 1$, in a bistable potential.

We start from the fractional Fokker-Planck equation (FFPE)

$$\frac{\partial f}{\partial t} = \frac{\partial}{\partial x} \left(\frac{dU}{dx} \frac{f}{m\gamma} \right) + D \frac{\partial^\alpha f}{\partial |x|^\alpha}, \quad (16)$$

for the density $f(x, t)$ to find the diffusing particle at position x at time t [15]. Here, the potential $U(x)$ is defined in Eq. (9a), and the fractional Riesz derivative $\partial^\alpha / \partial |x|^\alpha$ is understood via its Fourier transform,

$$\mathcal{F} \left\{ \frac{\partial^\alpha}{\partial |x|^\alpha} f(x, t) \right\} \equiv \int_{-\infty}^{\infty} e^{ikx} \frac{\partial^\alpha}{\partial |x|^\alpha} f(x, t) dx = -|k|^\alpha f(k, t). \quad (17)$$

We note that the FFPE (16) is equivalent to the Langevin approach in Eqs. (4) to (7).

After rescaling in the same way as outlined above, we arrive at the FFPE with dimensionless variables,

$$\frac{\partial f}{\partial t} = \frac{\partial}{\partial x} \left(\frac{dU}{dx} f \right) + D \frac{\partial^\alpha f}{\partial |x|^\alpha}, \quad (18a)$$

where

$$U(x) = -\frac{x^2}{2} + \frac{x^4}{4}. \quad (18b)$$

We can rewrite Eq. (18a) in terms of the flux j ,

$$\frac{\partial f}{\partial t} + \frac{\partial j}{\partial x} = 0. \quad (19)$$

We follow the stationary flux approximation of the Brownian theory, and also pursue the assumptions used to obtain the escape time in the Brownian limit [35], and can be justified in a more stringent approach [3]. Namely, we solve the stationary Eq. (16), under the assumption that the stationary distribution of particles differs significantly from the equilibrium distribution: the ‘‘source’’ ensures that all particles are on the left-hand side of the barrier, causing the steady influx of particles toward the barrier; after crossing it, the particles disappear through the ‘sink’. That is, following Ref. [35] we assume

$$\int_{-\infty}^0 f(x) dx = 1, \quad (20a)$$

and

$$j(x) = j_0 = T_{\text{esc}}^{-1}, \quad (20b)$$

where j_0 is the constant flux of particles across the barrier, and T_{esc} corresponds to the mean first passage time.

Transforming to Fourier space, the FFPE becomes

$$\frac{\partial f}{\partial t} = k \frac{\partial f}{\partial k} + k \frac{\partial^3 f}{\partial k^3} - D|k|^\alpha f(k), \quad (21)$$

while Eq. (19) attains the form

$$\frac{\partial f}{\partial t} - ikj(k) = 0. \quad (22)$$

Comparing Eqs. (21) and (22), we obtain for the Fourier transform of the flux the expression

$$j(k) = -i \frac{\partial^3 f}{\partial k^3} - i \frac{\partial f}{\partial k} + i D \text{sign}(k) |k|^{\alpha-1} f. \quad (23)$$

Now, with the use of Eq. (20b) it follows from Eq. (23) that the stationary solution in the constant flux approximation is determined by the following equation [36]:

$$\frac{d^3 f}{dk^3} + \frac{df}{dk} - D \text{sign}(k) f = 2\pi i j_0 \delta(k). \quad (24)$$

We solve Eq. (24) on the right and left semi-axes, and then match the solutions. The details are presented in Appendix B. This procedure yields

$$f(k) = \begin{cases} j_0 \frac{\pi}{2ab} \exp(z^* k), & k \geq 0, \\ j_0 \frac{\pi}{2ab} \exp(-zk), & k < 0 \end{cases}, \quad (25)$$

where the constants a and b , and z are given in Eqs. (B21). The inverse Fourier transform is indeed a PDF, namely

$$\begin{aligned} f(x) &= \int_{-\infty}^{\infty} e^{-ikx} f(k) \frac{dk}{2\pi} \\ &= \frac{j_0}{2ab} \Re \int_0^{\infty} e^{k(ix+z)} dk \\ &= \frac{j_0}{2b} \frac{1}{(x+b)^2 + a^2}. \end{aligned} \quad (26)$$

The last step is the normalization conditions given by Eq. (20a). After integrating Eq. (26),

$$\frac{j_0}{2ab} \left(\frac{\pi}{2} + \arctan\left(\frac{b}{a}\right) \right) = 1, \quad (27)$$

we arrive at the final expression for the mean escape time,

$$T_{\text{esc}} = \frac{\pi}{4ab} \left(1 + \frac{2}{\pi} \arctan\left(\frac{b}{a}\right) \right). \quad (28)$$

For $D \ll 1$, we obtain from Eqs. (B26) and (B27) the asymptotic result for the escape time

$$T_{\text{esc}} \approx \frac{\pi}{D}, \quad D \ll 1. \quad (29)$$

This result agrees with numerical simulations using the Lévy noise ξ_α as stochastic force, within the accuracy of about 12 per cent.

V. CONCLUSIONS

We consider symmetric Lévy flights within the entire domain of Lévy indices, $0 < \alpha < 2$, in three generic types of the potential wells: bistable potential, metastable potential, and truncated harmonic potential. As the basis for the numerical analysis we use the Langevin equation with the Lévy noise as source for the stochastic force, whereas for the analytical treatment we employ the space fractional Fokker-Planck equation. We obtain the following results.

Firstly, we demonstrated by extensive numerical analysis based on solving the Langevin equation the existence of *three* dynamic regimes in the barrier crossing behavior of a particle driven by Lévy noise, namely:

(i) The regime of low noise intensity D , displaying an algebraic dependence of the mean escape time on D through $T_{\text{esc}} \simeq C(\alpha)/D^{\mu(\alpha)}$. In this regime the nature of the Lévy noise with its characteristic property to allow for large outliers, plays an essential role and dominates the escape process. We showed that the exponent $\mu(\alpha)$ remains approximately constant, $\mu \approx 1$ for $0 < \alpha < 2$; close to $\alpha = 2$, it displays a divergence towards the exponential dependence on $1/D$ at $\alpha = 2$, the case of Gaussian noise. In this low noise intensity regime, we observe a monotonous increase of the escape time with increasing

α (keeping the noise intensity D fixed). The probability density of escape times decays exponentially.

(ii) The regime of intermediate noise intensity, in which the escape time is determined by the central part of probability distribution of the noise. This regime is characterized by the following features: The difference between the escape times for different Lévy indices significantly decreases, since in the central part all stable distributions are very similar to each other, as well as to the Gaussian distribution. Additionally, there is a non-monotonic dependence of the escape time with increasing α . However, the probability densities of escape times still decay exponentially.

(iii) The universal regime of high noise intensity, where the particle escapes with the first step (or in very few steps). The curves denoting the dependence of the escape time T_{esc} on noise intensity D collapse onto a single curve for all values of α (including the Gaussian limit).

Secondly, for the particular Cauchy case, $\alpha = 1$ we develop the kinetic theory of the escape over the barrier in a bistable potential. We start from the space fractional Fokker-Planck equation and use the assumption of a constant flux over the barrier. We find analytically the expression for the escape time, which at low noise intensities produces the result $T_{\text{esc}} \approx \pi/D$. This result agrees with numerical simulation within the accuracy of about 12 per cent.

Acknowledgments

We wish to thank V. Yu. Gonchar and T. Koren for their help with the simulations, and M. Lomholt for discussions. RM acknowledges partial funding through the Natural Sciences and Engineering Research Council (NSERC) of Canada, and the Canada Research Chairs programme.

Appendix A: SIMULATIONS DESCRIPTION

In this Appendix, we briefly outline our simulations strategy, in particular, how we simulate the white Lévy noise $\xi_\alpha(n)$. The corresponding generator is taken from [37]. We start by calculating the value

$$X = \frac{\sin(\alpha\gamma)}{(\cos\gamma)^{1/\alpha}} \left(\frac{\cos([1-\alpha]\gamma)}{W} \right)^{(1-\alpha)/\alpha}, \quad (\text{A1})$$

where γ is a random value uniformly distributed on the interval $(-\pi/2, \pi/2)$, W is an independent random variable with exponential distribution, and α is the Lévy index, $0 < \alpha \leq 2$.

The proof that the calculated variable X possesses a Lévy distribution function goes as follows. Firstly, let $0 < \alpha < 1$. While $\gamma > 0$, the expression for X may be

presented as

$$X = \left(\frac{a(\gamma)}{W} \right)^{(1-\alpha)/\alpha}, \quad (\text{A2})$$

where

$$a(\gamma) = \left(\frac{\sin\alpha\gamma}{\cos\gamma} \right)^{\alpha/(1-\alpha)} \cos([1-\alpha]\gamma). \quad (\text{A3})$$

Then

$$\begin{aligned} P(0 \leq X \leq x) &= P(0 \leq X \leq x, \gamma > 0) \\ &= P\left(0 \leq \left(\frac{a(\gamma)}{W}\right)^{1/\alpha-1} \leq x, \gamma > 0\right) \\ &= P\left(W \geq x^{-\alpha/(1-\alpha)} a(\gamma), \gamma > 0\right) \\ &\equiv \frac{1}{\pi} \int_0^{\pi/2} d\gamma \int_{a(\gamma)x^{\alpha/(1-\alpha)}}^{\infty} d\xi e^{-\xi} \\ &= \int_0^{\pi/2} d\gamma \exp\left(-x^{-\alpha/(1-\alpha)} a(\gamma)\right). \quad (\text{A4}) \end{aligned}$$

The latter expression, according to Ref. [38] is an integral representation of Lévy distribution.

In the case $1 < \alpha \leq 2$ analogous steps pertain, but now for the quantity $P(X \geq x, \gamma > 0)$. When $\alpha = 1$, the relation for X turns into $X = \tan\gamma$, that, is known to be a random value with Cauchy PDF. One does not need to consider the case $\gamma < 0$: it merely corresponds to negative X values.

The numerical simulation of T_{esc} as function of D is performed according to the following flowchart:

1. A ‘‘particle’’ is placed at the potential minimum;
2. A value of α is fixed;
3. The discrete-time Langevin equation (8) is iterated, until the particle reaches a definite coordinate, namely $x = 0$ for the bistable potential, $x = 10$ for the metastable potential, and $x = \pm 1$ for the truncated harmonic potential;
4. The event time $t = n\Delta t$ is stored;
5. Steps 3 and 4 are executed 10,000 times for each fixed value of D , and the average escape time calculated;

A similar procedure is used to simulate the escape time PDF $p(t)$, apart from taking the average. Explicitly:

1. The ‘‘particle’’ is placed at the potential minimum;
2. Some value of D is fixed;
3. Some value of α is taken;

4. The discrete-time Langevin equation (8) is iterated, until the ‘‘particle’’ reaches a definite coordinate, namely $x = 0$ for the bistable potential, $x = 10$ for the metastable potential, and $x = \pm 1$ for the truncated harmonic potential;
5. The event time $t = n\Delta t$ is stored;
6. Step 4 is executed 200,000 times for each fixed value of α , but, this time, the obtained event times are not averaged, but handled with a simple routine, that builds the PDF;

Each run was repeated and both results compared. Throughout, high reliability was observed.

Appendix B: MATCHING PROCEDURE

In this Appendix, we collect the necessary steps to identify the constants for the determination of the density f in the barrier crossing for the Cauchy case.

To this end, we solve Eq. (24) on the right and left semi-axes, and then match the solutions. For the two domains, we make the exponential ansatz

$$f(k) = \begin{cases} C_1 e^{zk} + C_2 e^{z^*k}, & k > 0; \\ C_3 e^{\zeta k} + C_4 e^{\zeta^*k}, & k < 0, \end{cases} \quad (\text{B1})$$

where

$$z = -\frac{u_+ + v_+}{2} + i\frac{u_+ - v_+}{2}\sqrt{3}, \quad (\text{B2})$$

with

$$u_+^3 = \frac{D}{2} \left[1 + \sqrt{1 + \frac{4}{27D^2}} \right], \quad (\text{B3a})$$

$$v_+^3 = \frac{D}{2} \left[1 - \sqrt{1 + \frac{4}{27D^2}} \right]. \quad (\text{B3b})$$

Moreover, we define

$$\zeta = -\frac{u_- + v_-}{2} + i\sqrt{3}\frac{u_- - v_-}{2}, \quad (\text{B4})$$

with

$$u_-^3 = \frac{D}{2} \left[-1 + \sqrt{1 + \frac{4}{27D^2}} \right] = -v_+^3, \quad (\text{B5a})$$

$$v_-^3 = \frac{D}{2} \left[-1 - \sqrt{1 + \frac{4}{27D^2}} \right] = -u_+^3, \quad (\text{B5b})$$

which implies that

$$\zeta = \frac{u_- + v_-}{2} + \frac{u_- - v_-}{2}i\sqrt{3}, \quad z^* = -\zeta. \quad (\text{B6})$$

To determine the unknown complex constants C_1, C_2, C_3, C_4 we match the results at $k = 0$. Thus,

firstly, we require $f(k - 0) = f(k + 0)$, which, using Eq. (B1) yields

$$C_1 + C_2 = C_3 + C_4. \quad (\text{B7})$$

The second condition is obtained by integration of Eq. (24) over the small region $[-\varepsilon, \varepsilon]$:

$$\int_{-\varepsilon}^{\varepsilon} dk f''' + \int_{-\varepsilon}^{\varepsilon} dk f' - D \int_{-\varepsilon}^{\varepsilon} dk \text{sign}(k) f = 2\pi i j_0. \quad (\text{B8})$$

In the limit $\varepsilon \rightarrow 0$ we recover the condition

$$f''(0+) - f''(0-) = 2\pi i j_0, \quad (\text{B9})$$

or, after inserting Eq. (B1) into Eq. (B9),

$$C_1 z^2 + C_2 z^{*2} - C_3 \zeta^2 - C_4 \zeta^{*2} = 2\pi i j_0. \quad (\text{B10})$$

The third condition is that the PDF is a real function:

$$f(x) = \int_0^{\infty} \frac{dk}{2\pi} e^{-ikx} f_1(k) + \int_{-\infty}^0 \frac{dk}{2\pi} e^{-ikx} f_2(k), \quad (\text{B11})$$

and

$$f^*(x) = \int_0^{\infty} \frac{dk}{2\pi} e^{ikx} f_1^*(k) + \int_{-\infty}^0 \frac{dk}{2\pi} e^{ikx} f_2^*(k). \quad (\text{B12})$$

On the other hand, by changing $k \rightarrow -k$ in Eq. (B11), we find

$$f(x) = \int_{-\infty}^0 \frac{dk}{2\pi} e^{ikx} f_1(-k) + \int_0^{\infty} \frac{dk}{2\pi} e^{ikx} f_2(-k). \quad (\text{B13})$$

Since $f(x)$ is a real function, we see from Eqs. (B12) and (B13):

$$f_1^*(k) = f_2(-k), \quad f_2^*(k) = f_1(-k). \quad (\text{B14})$$

Let us now insert Eq. (B1) into Eqs. (B14). From the first equation we have

$$C_1^* e^{z^*k} + C_2^* e^{z^*k} = C_3 e^{-\zeta k} + C_4 e^{-\zeta^*k}. \quad (\text{B15})$$

The second equation gives rise to the same result. Since $z^* = -\zeta$ (see Eq. (B6)), we have

$$C_1^* = C_3, \quad C_2^* = C_4. \quad (\text{B16})$$

Moreover, from Eqs. (B16) and (B7) we see that

$$(C_1 + C_2)^* = C_3 + C_4 = C_1 + C_2; \quad (\text{B17})$$

thus, from Eqs. (B16) and (B17), we obtain the following relations:

$$C_{1R} = C_{3R}, \quad C_{2R} = C_{4R}, \quad (\text{B18a})$$

$$C_{3I} = -C_{1I}, \quad C_{4I} = -C_{2I}, \quad (\text{B18b})$$

$$C_{2I} = -C_{1I}, \quad C_{4I} = -C_{3I}, \quad (\text{B18c})$$

$$C_{2I} = C_{3I} = -C_{1I} = -C_{4I}. \quad (\text{B18d})$$

Therefore, we are actually dealing with 3 constants only, namely, C_{1R} , C_{2R} and C_I :

$$C_1 = C_{1R} + iC_I, \quad C_2 = C_{2R} - iC_I, \quad (\text{B19a})$$

$$C_3 = C_{1R} - iC_I, \quad C_4 = C_{2R} + iC_I. \quad (\text{B19b})$$

Inserting Eqs. (B19) into Eq. (B10) produces

$$C_{1R}(z^2 - \zeta^2) + C_{2R}(z^{*2} - \zeta^{*2}) + iC_I(z^2 - z^{*2} + \zeta^2 - \zeta^{*2}) = 2\pi i j_0. \quad (\text{B20})$$

For convenience, we define

$$a = \frac{u_+ + v_+}{2}, \quad b = \frac{\sqrt{3}}{2}(u_+ - v_+). \quad (\text{B21})$$

Then

$$z = -a + ib, \quad \zeta = a + ib; \quad (\text{B22})$$

such that

$$z^2 - \zeta^2 = -4iab, \quad (\text{B23a})$$

$$z^{*2} - \zeta^{*2} = 4iab, \quad (\text{B23b})$$

$$z^2 - z^{*2} + \zeta^2 - \zeta^{*2} = 0. \quad (\text{B23c})$$

With the use of Eq. (B23) we get from Eq. (B20):

$$C_{2R} - C_{1R} = \frac{\pi j_0}{2ab}. \quad (\text{B24})$$

Now, combine Eqs. (B19) and (B24), and insert into Eqs. (B1):

$$f_1(k) = (C_{1R} + iC_I)e^{zk} + \left(C_{1R} + \frac{\pi j_0}{2ab} - iC_I\right)e^{z^*k}, \quad k \geq 0 \quad (\text{B25a})$$

$$f_2(k) = (C_{1R} - iC_I)e^{\zeta k} + \left(C_{1R} + \frac{\pi j_0}{2ab} + iC_I\right)e^{\zeta^*k}, \quad k < 0. \quad (\text{B25b})$$

We are looking for the stationary (non-equilibrium) distribution; therefore we assume $C_{1R} = C_I = 0$ in order to retain in Eq. (B25) only those terms, that are proportional to the flux j_0 . This leads us to the result (25).

To calculate the $D \ll 1$ limit of the characteristic escape time (29), we obtain the following limiting behaviours. Thus, from Eqs. (B3) and (B21) we see that

$$u_+ \approx \frac{1}{\sqrt{3}} \left(1 + \frac{\sqrt{3}D}{2}\right), \quad (\text{B26a})$$

$$v_+ \approx \frac{1}{\sqrt{3}} \left(-1 + \frac{\sqrt{3}D}{2}\right); \quad (\text{B26b})$$

and

$$a \approx D/2, \quad b \approx 1, \quad (\text{B27a})$$

$$\arctan\left(\frac{b}{a}\right) \approx \arctan\left(\frac{2}{D}\right) \approx \frac{\pi}{2}. \quad (\text{B27b})$$

Appendix C: COMPARISON TO ANALYTIC RESULTS FROM REF. [26]

In this Appendix, we show that our results are consistent with those obtained by Imkeller and Pavlyukevich from a different approach to the barrier crossing problem of a particle exposed to Lévy stable noise [26].

We recall that in Ref. [26], the authors start from the formula

$$\langle \exp(ik\mathfrak{L}_t) \rangle = \exp(-\mathfrak{C}(\alpha)t|k|^\alpha), \quad (\text{C1})$$

with $0 < \alpha < 2$, where \mathfrak{L}_t is the Lévy stable process in the Lévy-Khintchin representation. The constant \mathfrak{C} is defined as

$$\mathfrak{C}(\alpha) = 2 \int_0^\infty \frac{1 - \cos y}{y^{1+\alpha}} dy = \frac{2\Gamma(1-\alpha)}{\alpha} \cos\left(\frac{\pi\alpha}{2}\right) \quad (\text{C2})$$

for α strictly smaller than 2. In Ref. [26], the authors investigate the system driven by the Lévy stable process $\varepsilon\mathfrak{L}_t$, where ε corresponds to the noise intensity:

$$\langle \exp(ik\varepsilon\mathfrak{L}_t) \rangle = \exp(-\mathfrak{C}(\alpha)t\varepsilon^\alpha|k|^\alpha). \quad (\text{C3})$$

Note that ε is not completely equivalent to our noise intensity D . Indeed, in the main body of the paper we investigate the system as driven by the Lévy stable process L_t , with

$$\langle \exp(ikL_t) \rangle = \exp(-Dt|k|^\alpha). \quad (\text{C4})$$

Since $L_t = \varepsilon\mathfrak{L}_t$, from comparison of Eqs. (C4) and (C3), we see that

$$D = \mathfrak{C}(\alpha)\varepsilon^\alpha. \quad (\text{C5})$$

Consider the exemplaric case of the truncated harmonic potential

$$U(x) = \begin{cases} x^2/2, & -1 \leq x \leq 1 \\ 0, & \text{otherwise} \end{cases}. \quad (\text{C6})$$

From our formula $T_{\text{esc}} \simeq C(\alpha)/D^{\mu(\alpha)}$, assuming that $\mu(\alpha) \approx 1$ (that we found to be nicely fulfilled for small and intermediate values of α , see Fig. 3), we find that

$$T_{\text{esc}} \simeq C(\alpha)/D. \quad (\text{C7})$$

The result reported in Ref. [26] for this potential profile at small noise intensities behaves like

$$\mathfrak{T} \approx \frac{\alpha}{2\varepsilon^\alpha}, \quad (\text{C8})$$

see Eq. (24) from Ref. [26], with their constants a and b chosen as unity, $a = b = 1$.

Thus, if we require $T_{\text{esc}} = \mathfrak{T}$, then by virtue of Eqs. (C7), (C8), (C5), and (C2), we find the relation

$$C(\alpha) = \frac{\alpha}{2} \mathfrak{C}(\alpha) = \Gamma(1 - \alpha) \cos\left(\frac{\pi\alpha}{2}\right). \quad (\text{C9})$$

From this relation we find the asymptotic behavior of $C(\alpha)$,

$$C(\alpha) \approx \begin{cases} \Gamma(1) = 1, & \alpha \rightarrow 0, \\ \pi/2, & \alpha = 1 \\ 1/(2 - \alpha) \rightarrow \infty, & \alpha \rightarrow 2^- \end{cases}, \quad (\text{C10})$$

that agrees nicely with our numerical results, see Fig. 3 in the inset of the bottom graph corresponding to the truncated harmonic potential.

Fig.7 shows a direct comparison between the analytical result from Ref. [26] and our numerical results, by enforcing the $\mu(\alpha) = 1$ equality. The agreement is excellent. We also show that taking a variable $\mu(\alpha)$ into account, only a slight deviation is obtained.

For comparison, Fig. 8 shows the analogous results for the case of the bistable potential. While general agreement is quite good, for Lévy index decreasing below $\alpha = 1$, an increasing deviation is observed. We note that according to the results from Ref. [26], the coefficient C is π at $\alpha = 1$, in accordance with our result (29).

-
- [1] H. A. Kramers, *Physica A* **7**, 284 (1940).
[2] L. S. Pontryagin, A. A. Andronov, and A. A. Vitt, *Zh. Eksp. Teor. Fiz. (Soviet Phys. JETP)* **3**, 165 (1933).
[3] R. L. Stratonovich, *Topics of the Theory of Random Noise, Vol.II* (Gordon and Breach, New York, 1967).
[4] P. Hänggi, P. Talkner, and M. Bokrovec, *Rev. Mod. Phys.* **62**, 251 (1990).
[5] V. I. Mel'nikov, *Phys. Rep.* **209**, 1 (1991). Reaction rate problems
[6] S. Chandrasekhar, *Rev. Mod. Phys.* **15**, 1 (1943).
[7] H. Risken, *The Fokker-Planck equation* (Springer-Verlag, Berlin, 1989).
[8] J.-P. Bouchaud and A. Georges, *Phys. Rep.* **195**, 127 (1990).
[9] R. Metzler and J. Klafter, *J. Phys. A* **37**, R161 (2004).
[10] J. Klafter and M. F. Shlesinger, *Proc. Natl. Acad. Sci. U.S.A.* **83**, 848 (1986); A. Blumen, J. Klafter, and G. Zumofen, in *Optical Spectroscopy of Glasses*, edited by I. Zschokke (Reidel, Amsterdam, 1986).
[11] M. O. Vlad, R. Metzler, T. F. Nonnenmacher, and M. C. Mackey, *J. Math. Phys.* **37**, 2279 (1996).
[12] R. F. Grote and J. T. Hynes, *J. Chem. Phys.* **73**, 2715 (1980).
[13] P. Hänggi and F. Mojtabai, *Phys. Rev. A* **26**, 1168 (1982).
[14] R. Metzler and J. Klafter, *Chem. Phys. Lett.* **321**, 238 (2000).
[15] R. Metzler and J. Klafter, *Phys. Rep.* **339**, 1 (2000).
[16] H. Scher and E. W. Montroll, *Phys. Rev. B* **12**, 2455 (1975); G. Pfister and H. Scher, *Phys. Rev. B* **15**, 2062 (1977).
[17] J. Klafter, A. Blumen, and M. F. Shlesinger, *Phys. Rev. A* **35**, 3081 (1987).
[18] B. D. Hughes, *Random Walks and Random Environments*, Vol. 1: Random Walks (Oxford University Press, Oxford, 1995).
[19] V. Y. Gonchar, A. V. Chechkin, E. L. Sorokovoi, V. V. Chechkin, L. I. Grigor'eva, and E. D. Volkov, *Plasma Phys. Rep.* **29**, 380 (2003); O. G. Bakunin, *Plasma Phys. Rep.* **29**, 955 (2003); R. Jha, P. K. Kaw, D. R. Kulkarni, and J. C. Parikh, *Phys. Plasmas* **10**, 699 (2003); Y. Marandet, H. Capes, L. Godbert-Mouret, M. Koubiti, J. Rosato, and R. Stamm, *Euro. Phys. J. D* **39**, 247 (2006).
[20] I. M. Sokolov, J. Mai and A. Blumen, *Phys. Rev. Lett.* **79**, 857 (1997); D. Brockmann and T. Geisel, *Phys. Rev. Lett.* **91**, 048303; M. A. Lomholt, T. Ambjörnsson, and R. Metzler, *Phys. Rev. Lett.* **95**, 260603 (2005).
[21] H. Katori, S. Schlipf, and H. Walther, *Phys. Rev. Lett.* **79**, 2221 (1997).
[22] G. Zumofen and J. Klafter, *Chem. Phys. Lett.* **219** 303 (1994); E. Barkai and R. Silbey, *Chem. Phys. Lett.* **310**, 287 (1999).
[23] P. D. Ditlevsen, *Geophys. Res. Lett.* **26**, 1441 (1999).
[24] P. Lévy, *Théorie de l'addition des variables aléatoires* (Gauthier-Villars, Paris, 1954).
[25] B. V. Gnedenko and A. N. Kolmogorov, *Limit Distributions for Sums of Random Variables* (Reading, MA: Addison-Wesley, 1954).
[26] P. Imkeller and I. Pavlyukevich, *J. Phys. A* **39**, L237 (2006); P. Imkeller and I. Pavlyukevich, *Stochast. Proc. Applic.* **116**, 611 (2006).
[27] P. D. Ditlevsen, *Phys. Rev. E* **60**, 172 (1999).
[28] A. V. Chechkin, V. Yu. Gonchar, J. Klafter, R. Metzler, *Europhys. Lett.* **72**, 348 (2005).
[29] J.-D. Bao, H.-Y. Wang, Y. Jia, *Phys. Rev. E* **72**, 051105 (2005).
[30] A. V. Chechkin, V. Y. Gonchar, and M. Szydlowsky,

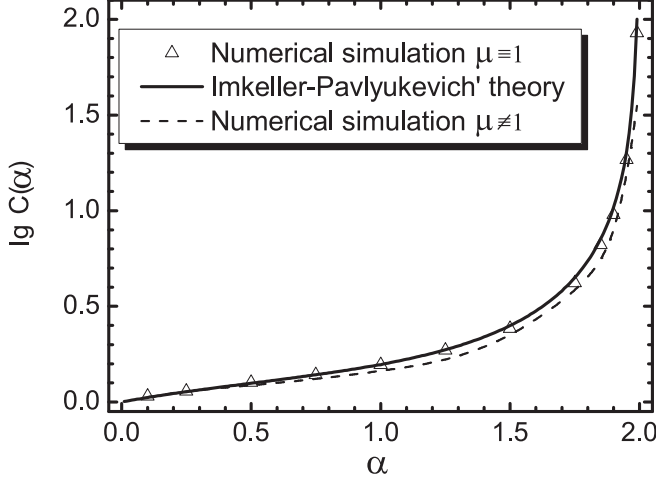


Figure 7: Comparison of the coefficients $C(\alpha)$ obtained by using numerical simulations with the analytical behaviour of $\mathcal{C}(\alpha)$ (full line) derived in Ref. [26], for the truncated harmonic potential. While the triangles denote our results for $\mu = 1$ fixed, the dashed line refers to our results with $\mu(\alpha)$, where we permit an explicit dependence on α .

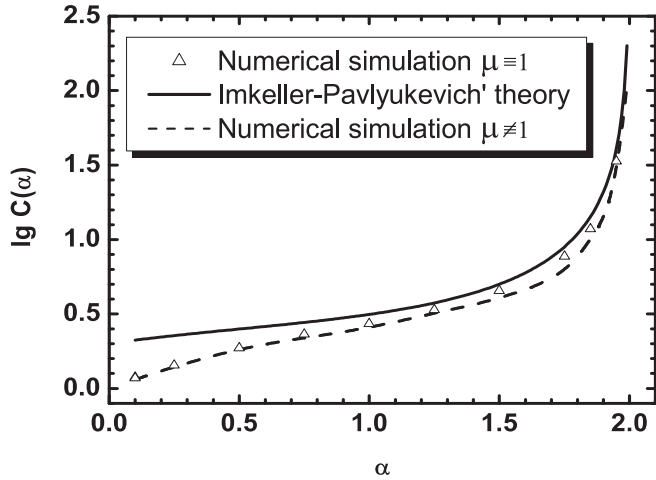


Figure 8: Comparison of the coefficients $C(\alpha)$ obtained by using numerical simulations with the analytical behaviour of $\mathcal{C}(\alpha)$ (full line) derived in Ref. [26], for the bistable potential.

Phys. Plasma **9**, 78 (2002); A. V. Chechkin and V. Yu. Gonchar, Zh. Eksp. Teor. Fiz. (JETP) **118**, 3, 730 (2000).

- [31] The simulation was performed in two ways: first, we used the programming language Borland C++ Builder 6 and, second, the symbolic mathematics package Mathematica 5. The step of time was taken equal to 0.01 in Borland C++ Builder program and 0.1 in simulation with Mathematica. The calculations made on Borland C++ Builder and Mathematica gave the same results (the accuracy was better than 0.7 percent). It was also proved that the simulation scheme is independent of the time quantization parameter (the inaccuracy did not exceed an error for the usual scheme of integrating an ordinary differential equation of first order by using the method of rectangles).
- [32] We note that in Fig. 2 the values of the noise intensity D for the Gaussian case is larger than the barrier height and thus Eq. (1) is not valid. Therefore, we here compare the result of numerical simulation with Eq. (44) from the treatise by Malakhov [33], which allows us to avoid the assumption of the high barrier. The corresponding theoretical curves are shown in Fig. 2 as bold lines for Levy index $\alpha = 2$. Obviously, there is excellent agreement between analytical solution given in Ref. [33] and the simulation results.
- [33] A. N. Malakhov, Chaos **7**, 488 (1997).
- [34] For the values of α and D shown in Fig. 4 the simulations were performed twice and the results compared. A good agreement was obtained, proving the reliability of the simulation.
- [35] Yu. L. Klimontovich, Statistical Theory of Open Systems, Vol. I (Kluwer Academic Publishers, Dordrecht, 1995).
- [36] Note that the Fourier transform of Eq. (20b) reads

$$j(k) = \int_{-\infty}^{\infty} j_0 e^{ikx} dx = 2\pi j_0 \delta(k). \quad (11)$$

- [37] J. M. Chambers et al., J. Americ. Statist. Assoc. **71**, 340 (1976).
- [38] V. M. Zolotarev, Moscow Mir, p. 187 (1983).